Volume 1 | Number 1 | Jan 2013 | Pages 1–100

Nanoscale

www.rsc.org/nanoscale

ROYAL SOCIETY
OF CHEMISTRY

ROYAL SOCIETY
OF CHEMISTRY

www.rsc.org/nanoscale

Journal Name

ARTICLE

Facile synthesis of luminescent and amorphous La₂O₃-ZrO₂ : Eu³⁺ nanofibrous membranes with robust softness

Weidong Han,[a] Bin Ding,*[c] Mira Park,[b] Fuhai Cui,[a] Zafar Khan Ghouri,[a] Prem Singh Saud,[a] and Hak-Yong Kim*[a]

Novel luminescent and amorphous La₂O₃-ZrO₂ : Eu³⁺ (LZE) nanofibrous membranes with robust softness are fabricated for the first time via a facile electrospinning technique. By employing zirconium oxide incorporation, the as-prepared lanthanum oxide nanofibrous membranes can be dramatically changed from the extreme fragility to robust softness. Meanwhile, the softness and luminescent performance of LZE nanofibrous membranes can be finely controlled by regulating the doping concentration of zirconium oxide and europium in lanthanum oxide nanofibers. Additionally, the crystal structure analysis using X-ray diffractometer and high resolution transmission electron microscopy measurements have confirmed the correlation between the amorphous structure and softness. Furthermore, LZE membranes show the characteristic emission of Eu³⁺ corresponding to $^5D_{0, 1, 2}$ - $^7F_{0, 1, 2, 3, 4}$ transitions due to an efficient energy transfer from O²⁻ to Eu³⁺. The LZE nanofibrous membranes with the optimum doping Eu³⁺ concentration of 3 mol%, the as-prepared LZE membranes exhibit excellent softness and luminescent properties, which make the materials have potential applications in fluorescent lamps and field emission displays.

Introduction

In recent years, many studies have been focused on the one dimensional (1D) nanomaterials, including nanowires,[1] nanorods,[2] and nanofibers,[3-5] due to their unique and fascinating characteristics and novel potential applications, such as high luminescence efficiency[6], superior mechanical toughness,[7, 8] and metal insulator transition.[9] There are several preparation methods to obtain 1D nanomaterials, such as vapor-phase transport process,[10] laser ablation,[11] and template based method.[12] However, most of these synthetic methods require either complex steps or expensive apparatuses, which severely restrict their use in large-scale production. In comparison to these methods, electrospinning is an effective and simple method for preparing nanofibers from a rich variety of materials, such as polymer,[8, 13, 14] inorganic,[15, 16] and hybrid compounds,[17, 18] which shows advantages of being energy-efficient, low cost, and easy to scale-up. Especially, inorganic nanofibers have attracted more and more attention due to their possessing high chemical and thermal stability, biocompatibility, and luminescence properties. Among the inorganic nanofibers, rare earth (RE) doped inorganic luminescent materials have

received startling interest because of their specific and fascinating properties, such as a high luminescence quantum yield, narrow emission bandwidth, and low toxicity, which can be widely used in the fields of field-emission display, biomedical[19], lighting,[20] etc. Eu³⁺ ion is one of the most frequently used red emitting activators in RE doped luminescent materials, which shows emission due to transition of $^5D_{0, 1, 2}$-^7F_J (J = 1, 2, 3, 4) in the orange-red regions.

Due to the thermal stability and high chemical stability of La₂Zr₂O₇, which can be used as hosts in RE luminescent materials. Some studies devoted to the synthesis of Ln³⁺ doped La₂Zr₂O₇ nano-/micrometer materials, and investigated their reaction mechanism, thermal stability, and luminescence properties. For example, Zhang and co-worker[21] reported about combustion method synthesis of La₂Zr₂O₇ : Eu³⁺, Dy³⁺ nanocrystals and studied the luminescence mechanism. Song and co-worker[22] used the hydrothermal route to synthesize La₂Zr₂O₇ : Eu³⁺ nanorods and investigate the photoluminescence properties. In fact, the commonly as-prepared Ln³⁺ doped La₂Zr₂O₇ luminescence materials are dominated in the form of phosphor powders, and only inhomogeneous nanoparticles or micro-sized particles were obtained, but also it is still a challenge to obtain uniformly dispersed nanostructures due to the nanoparticles have the tendency to aggregate, and the simple shape or construction limited their application fields to some extents. RE doped nanofibers may provide a better model system to investigate the dependence of electronic transport and optical properties on quantum size effects, and easy control the morphology of nanofibers. Meanwhile, nanofibrous-based luminescent membranes materials are stable and environmentally friendly better than powders-based materials. Liu and

[a.] Departement of BIN Fusion Technology, Chonbuk National University, Jeonju 561-756, Republic of Korea
[b.] Department of Organic Materials and Fiber Engineering, Chonbuk National University, Jeonju 561-756, Republic of Korea
[c.] Key Laboratory of Textile Science &Technology, Ministry of Education, College of Textiles, Donghua University, Shanghai 201620, China

worker fabricated $La_2Zr_2O_7 : Eu^{3+}$ nanofibers by electrospinning method and studied the photoluminescent properties[23]. However, a major shortfall of the electrospun inorganic membranes is that they are usually brittle or mechanically fragile to form freestanding overlaid mat, such a situation hinders their applications in many fields, such as flexible electronic devices,[24] supercapacitor,[25] and filtration/purification devices.[26, 27]

In view of the above situations, in this study, we demonstrated novel luminescent and amorphous La_2O_3-ZrO_2 : Eu^{3+} (LZE) nanofibrous membranes with excellent softness fabricated via electrospinning technique. The morphology and crystal structure of La_2O_3-ZrO_2 (LZ) and LZE membranes were investigated. Additionally, the softness of LZ and LZE membranes were controlled by the precursor nanofiber composition. Moreover, the luminous performance of the LZE membranes with different doped europium was also studied.

Experimental section

Chemicals and materials

Polyvinylpyrrolidone (PVP) (M_w = 1300 000), zirconium acetate solution (zirconium = 15-16 wt%), citric acid and europium nitrate pentahydrate were purchased from Sigma-Aldrich. Lanthanum nitrate hexahydrate was provided by Aladdin Co., Ltd. N, N-dimethylformamide (DMF) was obtained from Samchun Pure Chemical Co., Ltd. Ultra-pure water with a resistance of 18.2 MΩ was prepared by a water purification system. All the initial chemicals in this work were used without further purification.

Preparation

The stoichiometric amounts of lanthanum nitrate hexahydrate, citric acid (citric acid as a chelating agent for the metal ions, the molar ratio of metal ions to citric acid was 1 : 1) and different amounts of zirconium acetate solution were dissolved in DMF. The above solution was stirred for 4 h, after a certain amount of PVP was added to adjust the viscosity, with a 10 wt% in the DMF solution. Then, the solution was stirred for 12 h to form a homogeneous hybrid sol for further electrospinning. The as-prepared gel was loaded into a plastic syringe and connected to a high voltage power supply for electrospinning. A high voltage of 20 kV was applied between the spinneret and the collector at a gap of 15 cm. In this way, hybrid precursor nanofibrous membranes were obtained. Finally, the as-prepared precursor nanofibrous membranes were heated at a heating rate of 2 °C min^{-1} to 650°C, and hold 4 h in air. Various La_2O_3-ZrO_2 nanofibrous membranes were obtained, which were named as LZ-m (m corresponds to molar percentage of Zr/La : 0, 20, 40, and 60, respectively). On the basis of soft LZ-60 nanofibrous membranes, different amounts of europium nitrate pentahydrate was added to above hybrid sol, the as-prepared hybrid precursor membranes were processed similar above. The obtained LZE nanofibrous membranes were named as LZE-n (n corresponds to molar percentage of Eu^{3+} in La_2O_3 : 0.5, 1, 3, and 5, respectively).

Characterization

The morphology of the samples were inspected using a field emission scanning electron microscope (FE-SEM, Hitachi S-4700) and high resolution transmission electron microscopy (HR-TEM, JEOL JEM-2200FS) instrument with a field emission gun operating at 200 kV, energy dispersive X-ray spectroscopy (EDS) analysis was carried out on the HR-TEM as well. The X-ray diffraction patterns of the samples were carried out on an X-ray diffractometer (XRD, PANalytical X′ Pert-PRO) with a Cu Kα-ray (λ = 0.15405 nm). The photoluminescence measurements were recorded with a Fluorescence Spectrometer (PerkinElmer LS-55) equipped with a xenon lamp as the excitation source. All the measurements were performed at room temperature.

Results and discussion

To investigate the LZ nanofibrous membranes, the morphology of the membranes was firstly revealed from FE-SEM and optical images, which are shown in Fig. 1. Fig. 1a presents typical images of the LZ-0 membranes, which clearly showed that the nanofibers exhibited a fractured fiber morphology. Meanwhile, the membranes were in a powder form and showed extreme fragility. When the zirconium content in LZ membranes was 60 mol%, the LZ-60 membranes became soft during the bending process. Compared with the LZ-0, LZ-20, and LZ-40 membranes (the fractured nanofibers marked with yellow circle), the LZ-60 membranes showed robust softness and perfect fiber morphology, which reveal that the morphology and softness greatly changes with increasing amounts of zirconium. Moreover, Fig. S1 shows the EDS spectrums of LZ-0, LZ-20, LZ-40, and LZ-60 membranes, and the molar percentage of Zr/La : LZ-0 : 0%, LZ-20 : 16.70% , LZ-40 : 36.67%, and LZ-60 : 57.24%. Consequently, the above results show that the amounts of zirconium of 60 mol% for LZ membranes offers excellent softness, which could be applied as the optimum the amounts of zirconium. These results suggest that zirconium play an important role in determining the morphology and softness of LZ membranes. Due to the LZ-60 membranes exhibited an
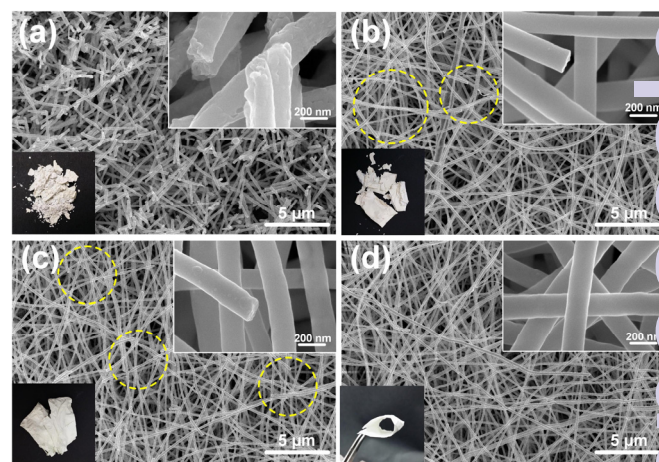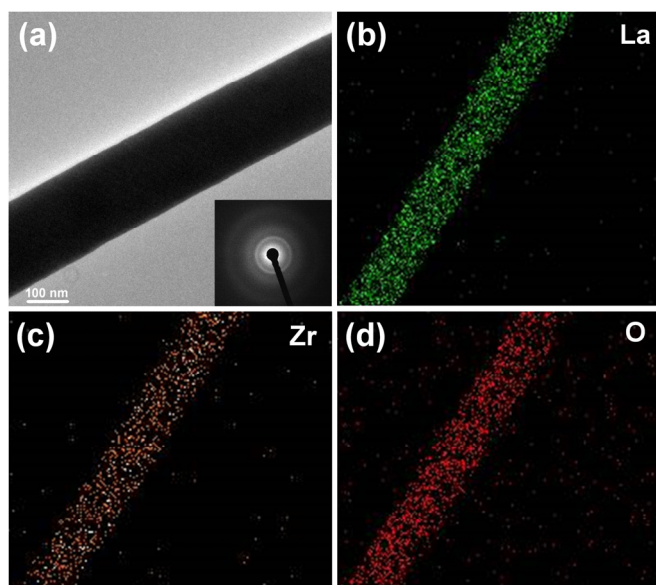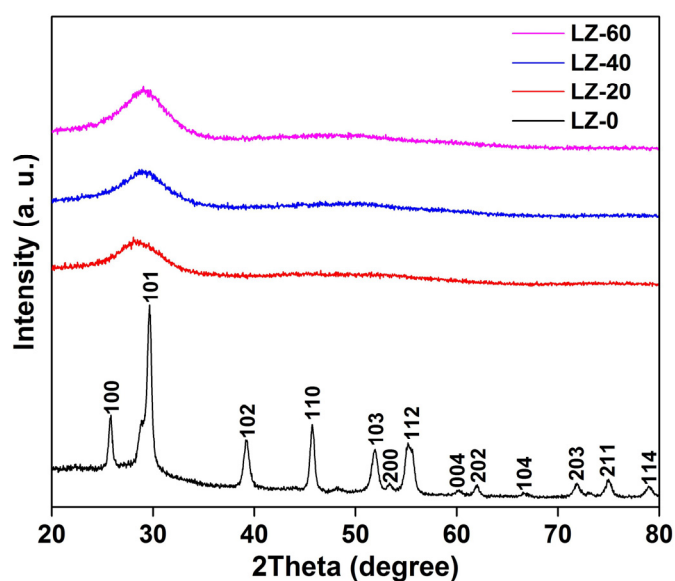

Fig. 1 FE-SEM images of (a) LZ-0, (b) LZ-20, (c) LZ-40, and (d) LZ-60 nanofibrous membranes. The insets are the optical images and magnified images of the corresponding nanofibrous membranes.

ARTICLE

Fig. 2 TEM image of the fabricated LZ-60 nanofibrous membranes. EDS mapping images of the LZ-60 nanofibers with (b) La element, (c) Zr element, and (d) O element. The insets are the corresponding SAED pattern.

excellent softness and perfect fiber morphology compared with the other membranes. Therefore, the shape and microstructure of the LZ-60 nanofibers are further examined by HR-TEM, and its elements composition are investigated by EDS. HR-TEM image of the LZ-60 nanofibers shows smooth without obvious pores and cracks (Fig. 2a). The dense structure of the nanofibers favors the improvement of the mechanical properties. The SEAD patterns of LZ-60 membranes exhibit a main halo peak without a sharp diffraction peak, indicating a fully glassy structure of the samples under a sensitivity of XRD (inset of Fig. 2a). Meanwhile, the amorphous feature was confirmed by HR-TEM imaging, as shown in Fig. 2a, from which no lattice orientation was observed. A EDS mapping scan was carried out to investigate the element distribution in the nanofibrous membranes (Fig. 2b-c). The obtained images show uniform

Fig. 3 XRD patterns of LZ-0, LZ-20, LZ-40, and LZ-60 nanofibrous membranes.
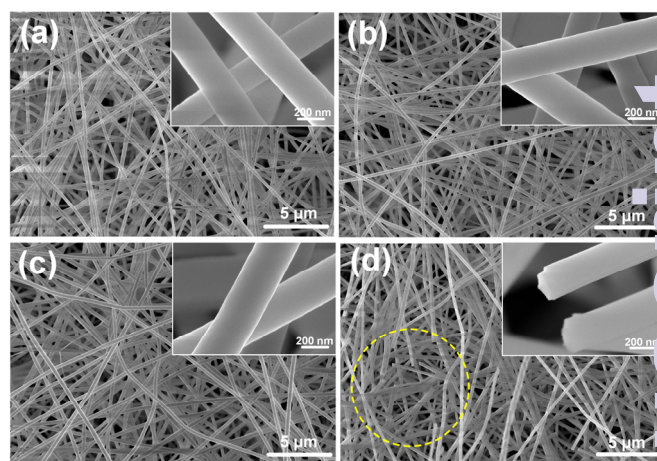
Fig. 4 FE-SEM images of (a) LZE-0.5, (b) LZE-1, (c) LZE-3, and (d) LZE-5 nanofibrous membranes. The insets are the magnified images of the corresponding nanofibrous membranes.

distributions of La, Zr, and O across the whole nanofibers.

The XRD patterns from 20° to 80° of LZ-0, LZ-20, LZ-40 and LZ-60 membranes are displayed Fig. 3. It clearly reveals that the doped zirconium of LZ-20, LZ-40 and LZ-60 membranes all belong to completely amorphous state, without any detectable crystalline Bragg peaks, it only shows a broad band at $2\theta=28°$, consistent with the electron diffraction pattern and XRD pattern. However, the XRD patterns of LZ-0 nanofibrous membranes indicate that the product calcined is crystallization, such (100), (101), and (102) can be recognized clearly, indicating the formation of lanthanum oxide with a fluorite structure, it was confirmed the crystallization of the La_2O_3. The peaks were assigned based on the JCPDS data (Powder Diffrction Card, # 05-0602 for La_2O_3). It indicates that the precursor sample has fully crystallized into La_2O_3 at this heating temperature.

Meanwhile, the morphologies and structure of the LZE nanofibrous membranes are characterized by FE-SEM. Typical FE-SEM images of LZE-0.5, LZE-1, LZE-3, and LZE-5 membranes are shown in Fig. 4, with a magnified image in the inset. From images of Fig. 4 and magnified micrograph, the LZE-0.5, LZE-1, and LZE-3 nanofibers shows uniform and smooth surface without obvious cracks, and diameters ranging from 160-340 nm. No obvious changes on the morphologies of LZE nanofibrous membranes with different europium content from 0.5 to 3 mol% can be observed (Fig. 4a-c), but it show that

Fig. 5 Photographs of LZ-0, LZE-0.5, LZE-1, LZE-3, and LZE-5 nanofibrous membranes. (a) The pictures were taken under white light. (b) The pictures were taken in a dark room by using a 254 nm ultraviolet lamp as excitation source.

LZE-5 sample have an evident increase of the fractured nanofibers from Fig. 4d (the fractured nanofibers marked with yellow circle). Fig. S2 shows the EDS spectrums of LZE-0.5, LZE-1, LZE-3, and LZE-5 membranes, and the molar percentage of Eu/(La+Eu) : LZE-0.5 : 0.32%, LZE-1 : 0.71%, LZE-3 : 2.30%, and LZE-5 : 4.15%. As shown in Fig. 5 are optical images of as-prepared LZE-0, LZE-0.5, LZE-1, LZE-3, and LZE-5 nanofibrous membranes under white light and a 254 nm ultraviolet lamp as excitation source. Red color luminescence of LZE membranes could be clearly observed under UV lamp. Further studies showed that the XRD patterns from 20º to 80º of LZE-0.5, LZE-1 LZE-3 and LZE-5 nanofibrous membranes are amorphous phase. The XRD pattern exhibits characteristic broad diffraction maxima without any detectable crystalline Bragg peaks (Fig. S3). The LZE-3 membranes was selected as a representative example to investigate photoluminescence properties. Fig. 6 shows the photoluminescence spectra of LZE-3 membranes. The excitation spectrum (Fig. 6a) monitored with 616 nm consists of an intense broad band from 200 to 350 nm. The strong broad band is due to the charge-transfer transition (CTB) between O^{2-} and Eu^{3+}. Excitation into the CTB transition of Eu^{3+} at 260 nm yields the emission spectrum (Fig. 6b) that consists of the emission lines from the $^5D_{0,1}$ excited states to the ^7F_J ground states of Eu^{3+}, i.e., $^5D_1$-$^7F_1$ (535 nm), $^5D_0$-$^7F_1$ (588 nm), $^5D_0$-$^7F_2$ (616 nm) and $^5D_0$-$^7F_4$ (702 nm), respectively. The emission spectrum is dominated by the hypersensitive red emission transition ($^5D_0$-$^7F_2$), indicating that the Eu^{3+} ions are located at sites without or deviating from inversion symmetry, which is consistent with the previous report[28].

The photoluminescence process of the LZE-3 nanofibrous membranes is shown in Fig. 7. For photoluminescence, electronic transitions from the O *2p* valence band to the La (*5d6s*) conduction band and charge-transfer from O^{2-} to Eu^{3+} occur under UV radiation excitation. After CTB excitation for Eu^{3+} doped LZ nanofibrous membranes most of the energy are transferred to the excited state $^5D_0$, $^5D_1$, $^5D_2$ levels of Eu^{3+},

Fig. 7 A scheme illumination the photoluminescence process in LZE-3 nanofibrous membranes.

which then return to the respective ground states and g... characteristic transitions of Eu^{3+}.

The photoluminescence intensity of the LZE membranes wa... depended on the Eu^{3+} ions concentration, which is shown in Fig. 8. Firstly, the photoluminescence intensity of Eu^{3+} increase... with increasing of the concentration, which reaching ... maximum value at 3 mol%, then decreased with the increase ... the concentration due to the concentration quenching effect. I... the energy migration among the activator ions at the high
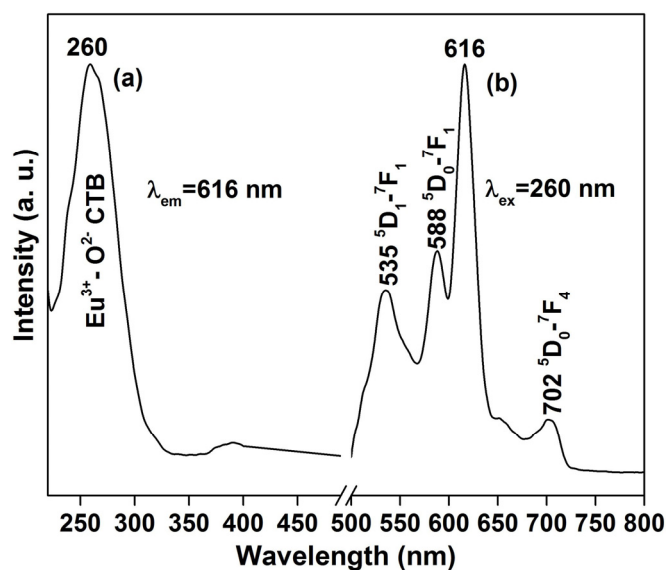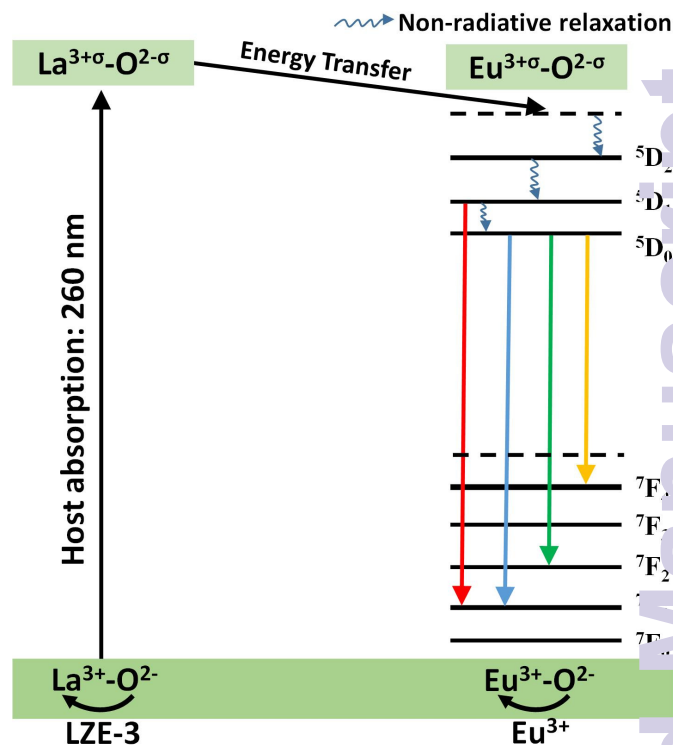

Fig. 6 The photoluminescence (a) excitation and (b) emission spectra of LZE-3 nanofibrous membranes.
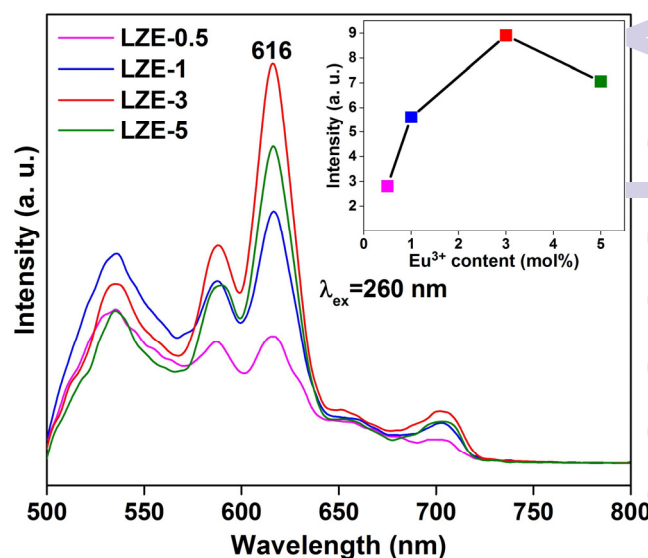

Fig. 8 The photoluminescence emission spectra of LZE-0.5, LZE-1, LZE-3 and LZE-5 nanofibrous membranes. The inset is the dependence of its photoluminescence intensity and the Eu^{3+} content in the LZE nanofibrous membranes.

Fig. 9 Luminescent photographs for LZE-3 nanofibrous membranes. The pictures were taken in a dark room by using a 254 nm ultraviolet lamp as excitation source. (a) Photograph depicting the mechanical softness of LZE-3 membranes. (b) The "Pentagram" pattern. (c) The "EXIT" pattern.

concentrations. In the energy migration process the excitation energy will be lost at a killer or quenching site, resulting in the decrease of photoluminescence intensity.[29] Thus, the optimum content of Eu^{3+} for LZE membranes is 3 mol% (LZE-3). It can clearly found that this result consistent with optical picture in Fig. 5b. Meanwhile, it can be seen that the LZE-3 nanofibrous membranes is easily bendable due to its excellent softness and can be readily cut to a desired shape (Fig. 9), indicating that the LZE-3 membranes could be used in luminescent patterning and related applications.

As shown in Fig. 10 the corresponding CIE chromaticity diagram of the photoluminescence colors for LZE-0.5, LZE-1, LZE-3, and LZE-5 nanofibrous membranes. The corresponding luminescence color can be tuned from orange-red by changing the doping concentrations of Eu^{3+} in LZE nanofibrous membranes. The various shapes indicated the CIE chromaticity coordinate positions. The CIE chromaticity coordinates change from x = 0.4423, y = 0.5398 for LZE-0.5 to x = 0.51, y = 0.4794 for LZE-5 by changing the doping concentration of Eu^{3+} from 0.5 to 5 mol% nanofiber phosphors. The corresponding
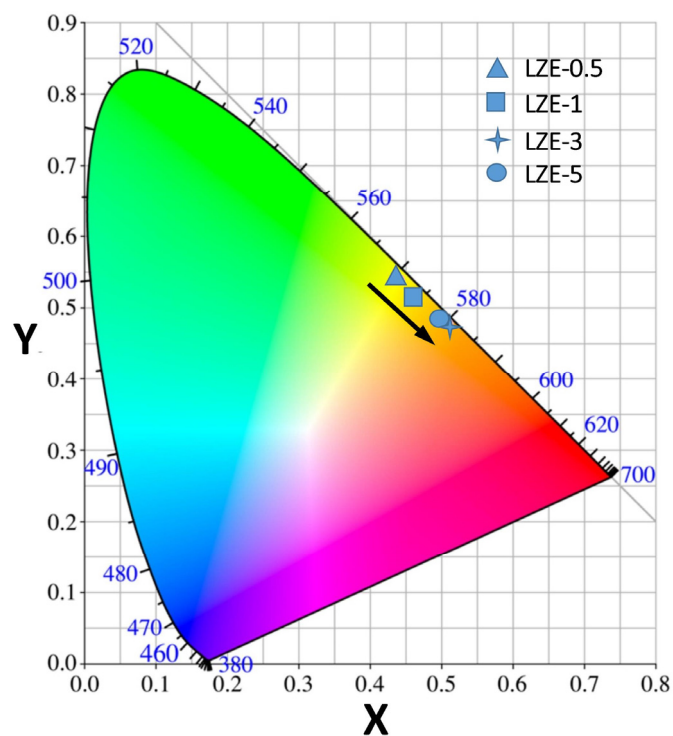
Fig. 10 CIE chromaticity diagram of LZE-0.5, LZE-1, LZE-3 and LZE-5 nanofibrous membranes.

luminescence color can be changed from orange-red, which can be seen clearly from the photographs of the LZE nanofibrous membranes presented in Fig. 5b.

The softness of LZ and LZE membranes have amorphous distribution, which have no long-range order, and only a short range order.[30] The disorder in atomic positions leads to emergent phenomena, and produce physical properties very different from their crystalline counterparts. The mechanism of the LZ and LZE membranes with excellent softness is associated with the nanostructure, and it been attributed to the interplay of local structure and bonding configuration in the voronoi network.[31] On the atomistic level, the structure of metal-metalloid and metal-metal in LZ and LZE membranes can be described as a space filling network of polyhedral.[30] According to this model, the centers of atomic clusters are occupied by the metalloid atoms. The atomic clusters are either connected by intercluster metal-metal bonds, or by sharing the metal atom to form edge-sharing or face-sharing cluster pairs. For that reason, the thermal stability and mechanical properties of and LZE nanofibers are determined by the interplay of the amorphous network. By chemically tuning the strengths and local arrangements of the interatomic interactions in the amorphous network, the shear modulus may be reduced resulting in an increase of the Poisson's ratio which enhance the softness of LZ and LZE membranes.

Conclusions

In summary, we have successfully synthesized novel luminescent and amorphous La_2O_3-ZrO_2 : Eu^{3+} nanofibrous membranes with robust softness by electrospinning method. The softness of LZ and LZE nanofibrous membranes exhibited a strong dependence on the zirconium and europium content respectively. The results of XRD and TEM indicate that the soft nanofibrous membranes show amorphous state. The as prepared LZE-3 nanofibrous membranes exhibit robust softness and excellent luminescent properties, suggesting their use as promising luminescent material for fluorescent lamps and field emission displays. This work also provided a versatile strategy for further design and development of soft inorganic nanofibrous membranes towards various applications.

Acknowledgements

Notes and references

1   M. H. Huang, S. Mao, H. Feick, H. Yan, Y. Wu, H. Kind, E. Weber, R. Russo and P. Yang, *Science*, 2001, **292**, 1897-1899.

2   X. Guo, W. Ye, H. Sun, Q. Zhang and J. Yang, *Nanoscale*, 2013, **5**, 12582-12588.

3   Z. Zhang, C. Shao, X. Li, Y. Sun, M. Zhang, J. Mu, P. Zhang, Z. Guo and Y. Liu, *Nanoscale*, 2013, **5**, 606-618.

4   D. Hou, W. Luo, Y. Huang, C. Y. Jimmy and X. Hu, *Nanoscale*, 2013, **5**, 2028-2035.

5   X. Zhang, V. Thavasi, S. G. Mhaisalkar and S. Ramakrishna, *Nanoscale*, 2012, **4**, 1707-1716.

6   G. Li, Z. Hou, C. Peng, W. Wang, Z. Cheng, C. Li, H. Lian and J. Lin, *Adv. Funct. Mater.*, 2010, **20**, 3446-3456.

7   E. Ozden, Y. Z. Menceloglu and M. Papila, *ACS Appl. Mater. Interfaces,* 2010, **2**, 1788-1793.

8   D. Papkov, Y. Zou, M. N. Andalib, A. Goponenko, S. Z. Cheng and Y. A. Dzenis, *ACS Nano*, 2013, **7**, 3324-3331.

9   C. Li, N. Chartuprayoon, W. Bosze, K. Low, K. H. Lee, J. Nam and N. V. Myung, *Electroanalysis*, 2014, **26**, 711-722.

10 R. B. Saunders, S. Garry, D. Byrne, M. O. Henry and E. McGlynn, *Cryst. Growth Des.*, 2012, **12**, 5972-5979.

11 L. Xin, Q. Shi, J. Chen, W. Tang, N. Wang, Y. Liu and Y. Lin, *Mater. Charact.*, 2012, **65**, 55-61.

12 S. H. Choi, D. Hwang, D. Y. Kim, Y. Kervella, P. Maldivi, S. Y. Jang, R. Demadrille and I. D. Kim, *Adv. Funct. Mater.*, 2013, **23**, 3146-3155.

13 J. Wang, Y. Li, H. Tian, J. Sheng, J. Yu and B. Ding, *RSC Adv.*, 2014, **4**, 61068-61076.

14 D. Grafahrend, K.-H. Heffels, M. V. Beer, P. Gasteier, M. Möller, G. Boehm, P. D. Dalton and J. Groll, *Nat. Mater.*, 2011, **10**, 67-73.

15 Y. Si, X. Mao, H. Zheng, J. Yu and B. Ding, *RSC Adv.*, 2015, **5**, 6027-6032.

16 N. Zhang, Y. Deng, Q. Tai, B. Cheng, L. Zhao, Q. Shen, R. He, L. Hong, W. Liu and S. Guo, *Adv. Mater.*, 2012, **24**, 2756-2760.

17 Y. Si, J. Yu, X. Tang, J. Ge and B. Ding, *Nat. Commun.*, 2014, **5**, 1-9.

18 V. Maneeratana, J. D. Bass, T. Azaïs, A. Patissier, K. Vallé, M. Maréchal, G. Gebel, C. Laberty-Robert and C. Sanchez, *Adv. Funct. Mater.*, 2013, **23**, 2872-2880.

19 Z. Hou, C. Li, P. a. Ma, Z. Cheng, X. Li, X. Zhang, Y. Dai, D. Yang, H. Lian and J. Lin, *Adv. Funct. Mater.*, 2012, **22**, 2713-2722.

20 Y. Gu, Q. Zhang, H. Wang and Y. Li, *J. Mater. Chem.*, 2011, **21**, 17790-17797.

21 A. Zhang, M. Lü, G. Zhou, S. Wang and Y. Zhou, *J. Phys. Chem. Solids*, 2006, **67**, 2430-2434.

22 H. J. Song, L. Q. Zhou, Y. Huang, L. Li, T. Wang and L. Yang, *Chin. J. Chem. Phys.*, 2013, **26**, 83-87.

23 R. Liu, X. Dong, J. Wang, W. Yu and G. Liu, *J. Optoelectron. Adv. Mater.*, 2014, **16**, 542-546.

24 H. Wu, L. Hu, M. W. Rowell, D. Kong, J. J. Cha, J. R. McDonough, J. Zhu, Y. Yang, M. D. McGehee and Y. Cui, *Nano Lett.*, 2010, **10**, 4242-4248.

25 M. S. Kolathodi and T. S. Natarajan, *Scr. Mater.*, 2015.

26 Q. Wen, J. Di, Y. Zhao, Y. Wang, L. Jiang and J. Yu, *Chem. Sci.*, 2013, **4**, 4378-4382.

27 Y. Chen, X. Mao, H. Shan, J. Yang, H. Wang, S. Chen, F. Tian, J. Yu and B. Ding, *RSC Adv.*, 2014, **4**, 2703-2710.

28 P. Dorenbos, *J. Alloy. Compd.*, 2009, **488**, 568-573.

29 O. Meza, E. Villabona-Leal, L. A. Diaz-Torres, H. Desirena, J. Rodríguez-López and E. Pérez, *J. Phys Chem. A*, 2014, **118**, 1390-1396.

30 H. Sheng, W. Luo, F. Alamgir, J. Bai and E. Ma, *Nature*, 2006, **439**, 419-425.

31 E. D. Cubuk and E. Kaxiras, *Nano Lett.*, 2014, **14**, 4065-4070.